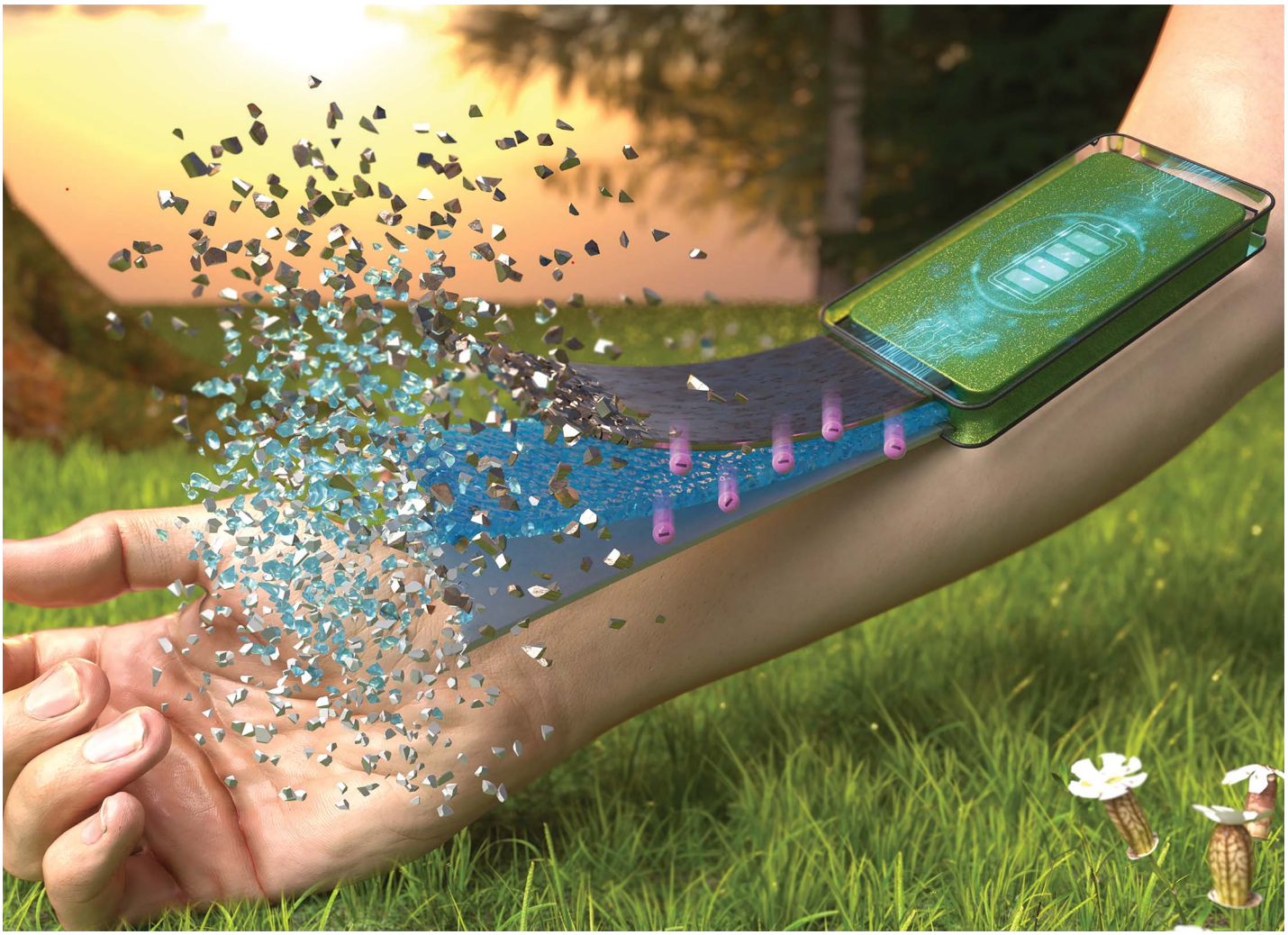

Showcasing research from Professor Suk-Won Hwang's laboratory, KU-KIST Graduate School of Converging Science and Technology, Korea University, Seoul, Republic of Korea.

Long-lasting, flexible and fully bioresorbable AZ31–tungsten batteries for transient, biodegradable electronics

Eco-friendly, biodegradable solid-state battery with a magnesium alloy anode, tungsten cathode, and alginate-based stretchable solid electrolytes offers stable output with high-corrosion resistance, ideal for sustainable flexible electronics.

As featured in:

See Jiung Cho, Suk-Won Hwang *et al.*, *J. Mater. Chem. A*, 2024, **12**, 32712.

ROYAL SOCIETY OF CHEMISTRY

rsc.li/materials-a

Registered charity number: 207890

Journal of Materials Chemistry A

ROYAL SOCIETY OF CHEMISTRY

PAPER

View Article Online
View Journal | View Issue

Check for updates

Cite this: J. Mater. Chem. A, 2024, 12, 32712

Long-lasting, flexible and fully bioresorbable AZ31–tungsten batteries for transient, biodegradable electronics†

Gwan-Jin Ko,‡[a] Tae-Min Jang, ‡[a] Daiha Shin,‡[b] Heeseok Kang, ‡[ac] Seung Min Yang,[d] Sungkeun Han, [a] Rajaram Kaveti,[ef] Chan-Hwi Eom,[a] So Jeong Choi,[a] Won Bae Han,[agh] Woon-Hong Yeo, [ghij] Amay J. Bandodkar, [ef] Jiung Cho*[k] and Suk-Won Hwang *[alm]

Received 2nd September 2024
Accepted 17th October 2024

DOI: 10.1039/d4ta06222a

rsc.li/materials-a

Rapid technological revolution produces a wide range of convenient tools, while, in particular, the production and consumption of batteries lead to various issues including environmental pollution. Although efforts to solve such problems increase interest in green and dissolvable batteries, their short service life is still recognized as a major obstacle due to limited options of materials. Here, we propose materials and system designs for eco-friendly and biodegradable magnesium alloy–tungsten (AZ31–W) batteries that offer long-term stability with enhanced corrosion resistance. Materials and electrochemical inspections confirm the superior electrochemical tolerance and stable, reliable potentials of the AZ31 anode and W cathode. The assembly of an individual cell into a commercially available pouch battery yields a high capacity of ~430 mA h g^{-1}, suitable for high-energy applications. The integration of alginate-based soft, elastic electrolytes with the electrodes enables the achievement of completely eco-resorbable solid-state batteries that maintain performance under diverse physical deformations. The results suggest potential for biomedical and eco-friendly applications where commercial batteries pose risks to the environment or human body.

1 Introduction

Innovative technologies that create new forms of materials, devices, and products such as transition from internal combustion engines to electric vehicles and from stationary to portable electronic systems, have brought about significant shifts in our lives, alongside challenges such as environmental pollution and global warming. One of the examples that are attracting people's attention at this time is an energy storage system, ranging from the well-known alkaline, lithium batteries to miniaturized or mechanically soft energy devices that can be applied to diverse types of wearable and implantable electronics.[1–8] Although existing components certainly provide stable power supply and high levels of performance, different approaches may need to be considered for system safety issues (*e.g.*, explosion) or biological/environmental impacts due to the potential release of toxic metals such as cobalt, nickel, and cadmium.[9–11] Consequently, research efforts towards environment-friendly and/or biodegradable battery systems in a solid-state format might be one of the ideal directions that

[a]KU-KIST Graduate School of Converging Science and Technology, Korea University, Seoul, 02841, Republic of Korea. E-mail: dupong76@korea.ac.kr
[b]Metropolitan Seoul Center, Korea Basic Science Institute (KBSI), Seoul, Republic of Korea
[c]Center for Advanced Biomolecular Recognition, Biomedical Research Division, Korea Institute of Science and Technology (KIST), Seoul, 02792, Republic of Korea
[d]Hanwha Systems Co., Ltd, Seongnam-si, Gyeonggi-do, 13524, Republic of Korea
[e]Department of Electrical and Computer Engineering, North Carolina State University, Raleigh, NC 27606, USA
[f]Center for Advanced Self-Powered Systems of Integrated Sensors and Technologies (ASSIST), North Carolina State University, Raleigh, NC 27606, USA
[g]George W. Woodruff School of Mechanical Engineering, Georgia Institute of Technology, Atlanta, GA 30332, USA
[h]IEN Center for Wearable Intelligent Systems and Healthcare, Georgia Institute of Technology, Atlanta, GA 30332, USA
[i]Wallace H. Coulter Department of Biomedical Engineering, Georgia Tech, Emory University School of Medicine, Atlanta, GA, 30332, USA
[j]Parker H. Petit Institute for Bioengineering and Biosciences, Institute for Materials, Institute for Robotics and Intelligent Machines, Georgia Institute of Technology, Atlanta, GA, 30332, USA
[k]Department of Materials Science and Engineering, Hongik University, Sejong, Republic of Korea. E-mail: jiungcho@hongik.ac.kr
[l]Department of Integrative Energy Engineering, Korea University, Seoul 02841, Republic of Korea
[m]Biomaterials Research Center, Korea Institute of Science and Technology (KIST), Seoul 02792, Republic of Korea

† Electronic supplementary information (ESI) available. See DOI: https://doi.org/10.1039/d4ta06222a

‡ These authors contributed equally to this work.

cannot be addressed by the conventional, established systems. Early and recent studies on such energy storage systems involved complete biodegradable batteries and supercapacitors using a pair of dissolvable metals as electrodes with liquid or solid-state electrolytes.[12–21] Some cases utilized partially degradable or non-degradable metals, but the entire systems were able to disappear through a series of small reactions or secondary products.[22,23] Although several examples have been proposed as prospective systems, the limited options of dissolvable metals available as electrodes, particularly the use of magnesium (Mg) as a typical anode material, resulted in a short operation life due to the low corrosion resistance.[24,25]

Here, we introduce environment-friendly, eco-resorbable battery systems in a soft and flexible format, using a magnesium alloy (AZ31) as an anode and tungsten (W) as a cathode. Utilizing the AZ31 magnesium alloy—an alloy known for its enhanced corrosion resistance compared to pure magnesium—improves the durability of the anode, while tungsten's corrosion resistance complements that of the AZ31 alloy, and serves as the cathode, contributing to the overall stability and longevity of the battery. Fundamental electrochemical inspections under diverse conditions indicate that the anodic alloy with low electrochemical potential and the cathode providing a large potential difference offer stable electrical potentials and strong chemical resistance over extended periods.[12,26,27] In addition, both the AZ31 magnesium alloy and tungsten are biocompatible and bioresorbable metals suitable for use in environmental and biomedical applications. The use of these biodegradable materials in a commercial pouch battery and the fabrication of a biodegradable solid-state battery highlight their potential as energy sources for wearable and implantable electronic systems.

2 Results and discussion

2.1 Eco-friendly, fully biodegradable solid-state battery

Fig. 1a represents series-connected degradable battery leaves that can power parallel-connected arrays of light-emitting diodes (LEDs). The eco-resorbable battery consists of a magnesium alloy (AZ31, 3% Al, 1% Zn) as an anode, tungsten (W) as a cathode, a soft and stretchable solid-state electrolyte (alginate composite electrolyte), and a packaging layer that isolates the electroactive materials from the external environment. The AZ31 alloy exhibits a high theoretical capacity and favorable biocompatibility similar to magnesium (Mg), with improved discharge characteristics due to enhanced corrosion resistance.[25–27] W, which has a large potential difference compared to Mg or Mg alloys and superior corrosion resistance, served as a cathode material suitable for a high-voltage and long-life biodegradable battery when combined with the AZ31 anode.[12,28,29] The solid-state electrolyte was composed of an alginate hydrogel with glycerol additives to enhance ionic conductivity and mechanical properties.[30] Together with a thin biodegradable polymer package (*e.g.*, poly(ε-caprolactone), PCL), a representative soft and flexible eco-resorbable battery was realized. Fig. 1b demonstrates natural biodegradation of the eco-resorbable battery components such as the AZ31 anode, W cathode, and stretchable electrolyte in soil under ambient temperatures. The result indicates that each component underwent gradual and harmless decomposition in the environment. Although the electrodes, with their stable corrosion resistance, maintained their morphological shapes over a 10 week period, they have also been verified to degrade and absorb in the soil, producing eco-friendly products over time, while the duration for complete degradation may vary depending on the soil environment.[26,31–34] We note that all constituent materials introduced in this study are bioresorbable and non-toxic, suggesting their potential for biomedical applications, while the long-term biocompatibility of these materials requires further detailed evaluation for practical uses.[33,35–41]

2.2 Electrochemical characteristics of anodic and cathodic materials

Metal electrodes in the galvanic series play key roles in properties including capacity, voltage, and energy/power density, particularly in bioresorbable batteries, the selection or combination of metals for each electrode is important. The diagram in Fig. 2a shows the electropotential series of dissolvable and noble metals for battery electrodes, against the standard silver/silver chloride (Ag/AgCl) electrode in phosphate buffered saline (PBS, pH 7) solution at room temperature. Mg (∼−1.6 V) and AZ31 (∼−1.55 V) exhibit the lowest electrochemical potential, suitable for use as an anode, while germanium (Ge, ∼−0.48 V), Mo (∼−0.31 V), Fe (∼−0.29 V), and W (∼−0.25 V) are appropriate for cathodes. Although Mg and AZ31 display similar potentials, reactive corrosion of Mg occurred significantly faster than that of AZ31 that has a high charge transfer resistance (R_{ct}) (Fig. S1†).[25,26] R_{ct} generally offers the advantage of stabilizing voltage output by controlling reaction rates and minimizing concentration polarization. In the case of AZ31, it regulates the dissolution and deposition processes of magnesium, ensuring consistent voltage levels and enhancing the stabilizing effects through interactions with alloying elements such as Al and Zn.[42–45] Fig. 2b presents the time-varying galvanic potential behaviors of each electrode when immersed in PBS solution (pH 7, RT). The AZ31 alloy (2 × 2 cm, 50 μm thick) maintained stable galvanic potentials against the standard Ag/AgCl electrode in 30 days, whereas Mg (2 × 2 cm, 50 μm thick) experienced rapid degradation and lost the functionality within 5 days, which is quite consistent with the properties of magnesium batteries reported in previous articles.[24,25] Fig. 2c (Mg) and Fig. 2d (AZ31) show cross-sectional scanning electron microscope (SEM) images before (left) and after (right) 24 h of immersion in PBS solution (pH 7, RT), and rapid reduction occurred in the Mg electrodes due to a self-corrosion reaction (see the cross-sectional SEM images for other time points in Fig. S2†). Temporal voltage profiles at various discharge currents of Mg (Fig. 2e) and AZ31 (Fig. 2f) indicate that the Mg electrode was stable for currents up to 100 μA cm^{-2}; however, it experienced a noticeable voltage drop at 1 mA cm^{-2}. In contrast, AZ31 maintained constant voltage levels even at 1 mA, presumably due to the high charge transfer resistance (see the time-dependent voltage profiles of AZ31 for other discharge current

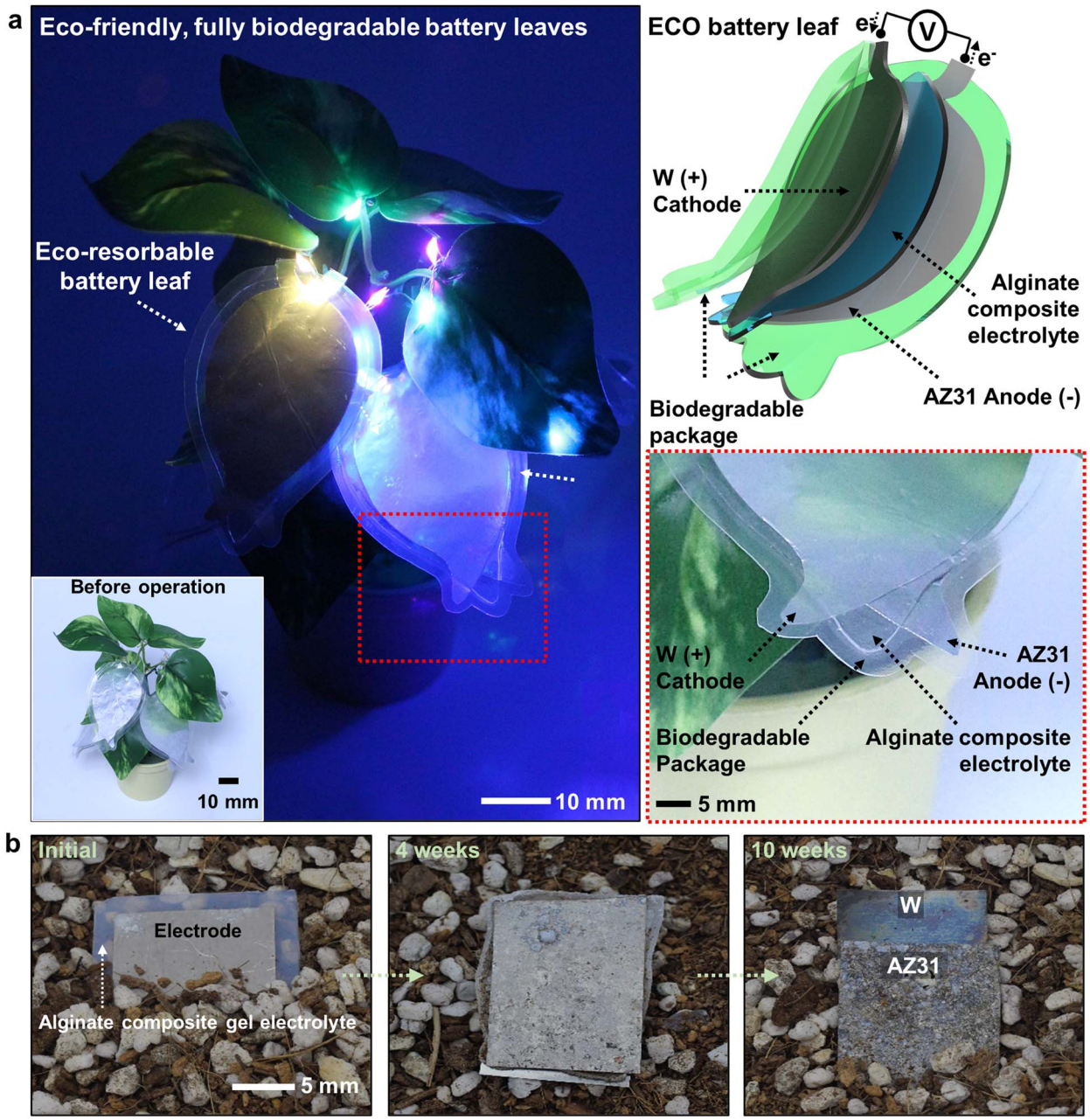

Fig. 1 Eco-friendly, fully biodegradable solid-state battery. (a) Representative image of the eco-friendly, bioresorbable solid-state battery leaves that enable the powering of microscale light-emitting diodes (μ-LEDs), with an image at an idle state in the inset. Each battery leaf consists of completely biodegradable materials, including tungsten (W) as a cathode, alginate composite gel as an electrolyte, a magnesium alloy (AZ31, 3% Al; 1% Zn) as an anode, and biodegradable packages (*e.g.*, polycaprolactone, PCL; polylactide, PLA; poly(L-lactide-*co*-ε-caprolactone), PLCL; poly(glycolide-*co*-ε-caprolactone), PGCL). (b) Collection of dissolution images of the degradable solid-state battery under environmental conditions (*e.g.*, soil), after 4 and 10 weeks.

densities and for other metals in Fig. S3 and S4†). Fig. 2g presents the potentiodynamic polarization curves of AZ31 and W electrodes measured in PBS electrolytes (pH 7, RT) within a voltage window of ~1.3 V. The results reveal that both materials remained in the active corrosion state across all tested current densities, which ensured a high operation voltage throughout the battery's lifecycle.[45] Fig. 2h illustrates the overall mechanism of an AZ31–W full cell, and the reaction of the Mg anode is as follows:

$$Mg \rightarrow Mg^{2+} + 2e^{-} \quad (1)$$

The following side reaction takes place simultaneously:

$$Mg + 2H_2O \rightarrow Mg(OH)_2 + H_2 \quad (2)$$

As for the W cathode, the reaction is assumed to be either oxygen reduction or hydrogen evolution.

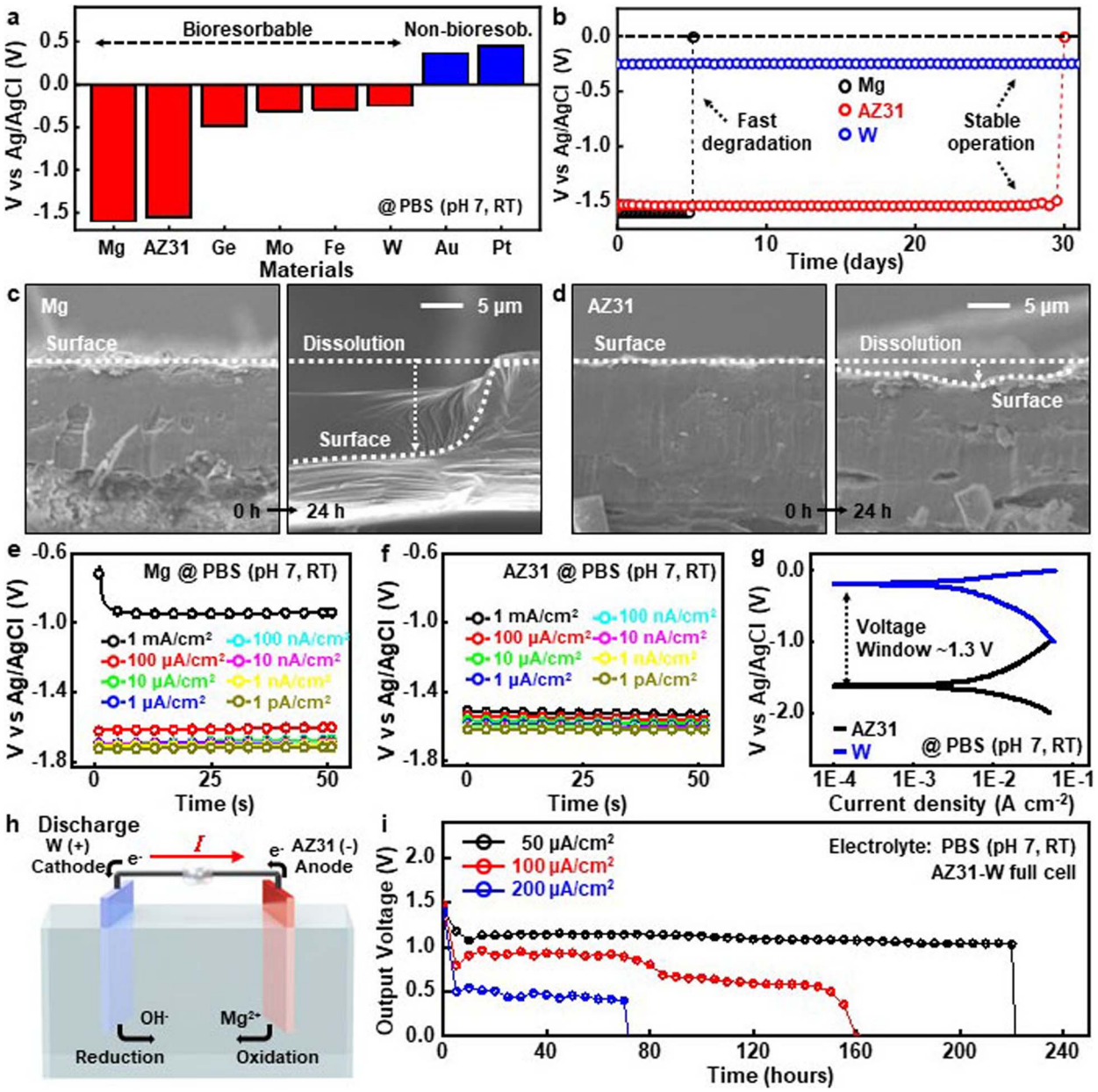

Fig. 2 Electrochemical characteristics of anodic and cathodic materials. (a) Galvanic potentials of bioresorbable metals as candidates (magnesium, Mg; magnesium aluminum zinc alloy, AZ31; germanium, Ge; molybdenum, Mo; iron, Fe; tungsten, W) and biocompatible novel metals (gold, Au; platinum, Pt) against standard reference electrodes (Ag/AgCl). (b) Time-dependent voltage profiles of AZ31 and Mg for anodes and W for a cathode as a potential candidate material. (c) and (d) Cross-sectional scanning electron microscopy (SEM) images of Mg (c) and AZ31 (d) anodes, after immersion in phosphate-buffered saline (PBS, pH 7.4) solution at room temperature for 0 (left) and 24 hours (right). (e) and (f) Measured electrode potentials of Mg (e) and AZ31 (f) against the standard reference electrode (Ag/AgCl) at various discharge current densities (100 pA cm^{-2} to 1 mA cm^{-2}). (g) Galvano-dynamic polarization of AZ31 and W, showing voltage profiles corresponding to different current densities. (h) Schematic illustration of an experiment set-up for an AZ31 (anode)–W (cathode) full cell in PBS solution (electrolyte). (i) Temporal output voltages of the galvanic cells at different discharge currents.

$$O_2 + 2H_2O + 4e^- \rightarrow 4OH^- \quad (3)$$

or

$$2H_2O + 2e^- \rightarrow H_2 + 2OH^- \quad (4)$$

The measured functional lifetime of the AZ31–W full cells in Fig. 2i were 225, 160, and 75 hours at discharge current densities of 50 (black), 100 (red), and 200 μA cm^{-2} (blue) in PBS electrolytes (pH 7, RT), which outperformed previously reported biodegradable batteries.[12,13,46] The stability of AZ31, particularly in terms of corrosion resistance and solubility, plays a crucial role in reducing side reactions such as oxidation products that decrease the reaction area of magnesium,[25,26] which contributes to the battery's long operation. Detail information about capacity at each discharge current is shown in Fig. S5.†

2.3 ECO pouch batteries

The deployment of the dissolvable metal electrodes in commercial battery products is one of the possible approaches to explore the practical feasibility of green energy storage devices. Fig. 3a displays a representative image of a dissolvable material-based eco-friendly (ECO) pouch battery with a biodegradable polymer package (*e.g.* poly ε-caprolactone, PCL). Individual electrochemical cells (AZ31 anodes, separator with PBS electrolytes, and W cathodes) were assembled into two series and three parallel connections to enhance overall battery performance (Fig. 3b). (The detailed circuit diagram is shown in Fig. S6.†) Fig. 3c illustrates the discharge behaviour of the pouch battery at a discharge current of 1 mA. Considering the electrode surface area (2 cm × 3 cm = 6 cm^2) and the series-parallel connection, this setup corresponds to a current density of 55 μA cm^{-2} per single cell. The resulting pouch cells exhibit a capacity of ~430 mA h g^{-1}, which is comparable to values reported in previous studies on non-degradable metal electrode-based primary batteries, highlighting the long-term performance of the dissolvable AZ31-based battery system.[47,48] (The voltage output of the ECO pouch battery over time under identical conditions is shown in Fig. S7.†) Fig. 3d showcases an array of 32 LEDs connected in parallel to form the letters 'ECO', powered by the home-made ECO pouch battery. The results demonstrate that the sufficient power with the high capacity enabled all the LEDs to operate for a prolonged duration of ~30 hours (Fig. 3e).

2.4 Soft, stretchable electrolytes for bioresorbable solid-state batteries

Several features of solid electrolytes including the electrochemical stability and mechanical flexibility which can solve or alleviate issues associated with conventional liquid electrolytes motivated research efforts to develop a solid-state degradable energy system. Fig. 4a illustrates a soft, bioresorbable solid-state battery with an alginate-based composite electrolyte using the

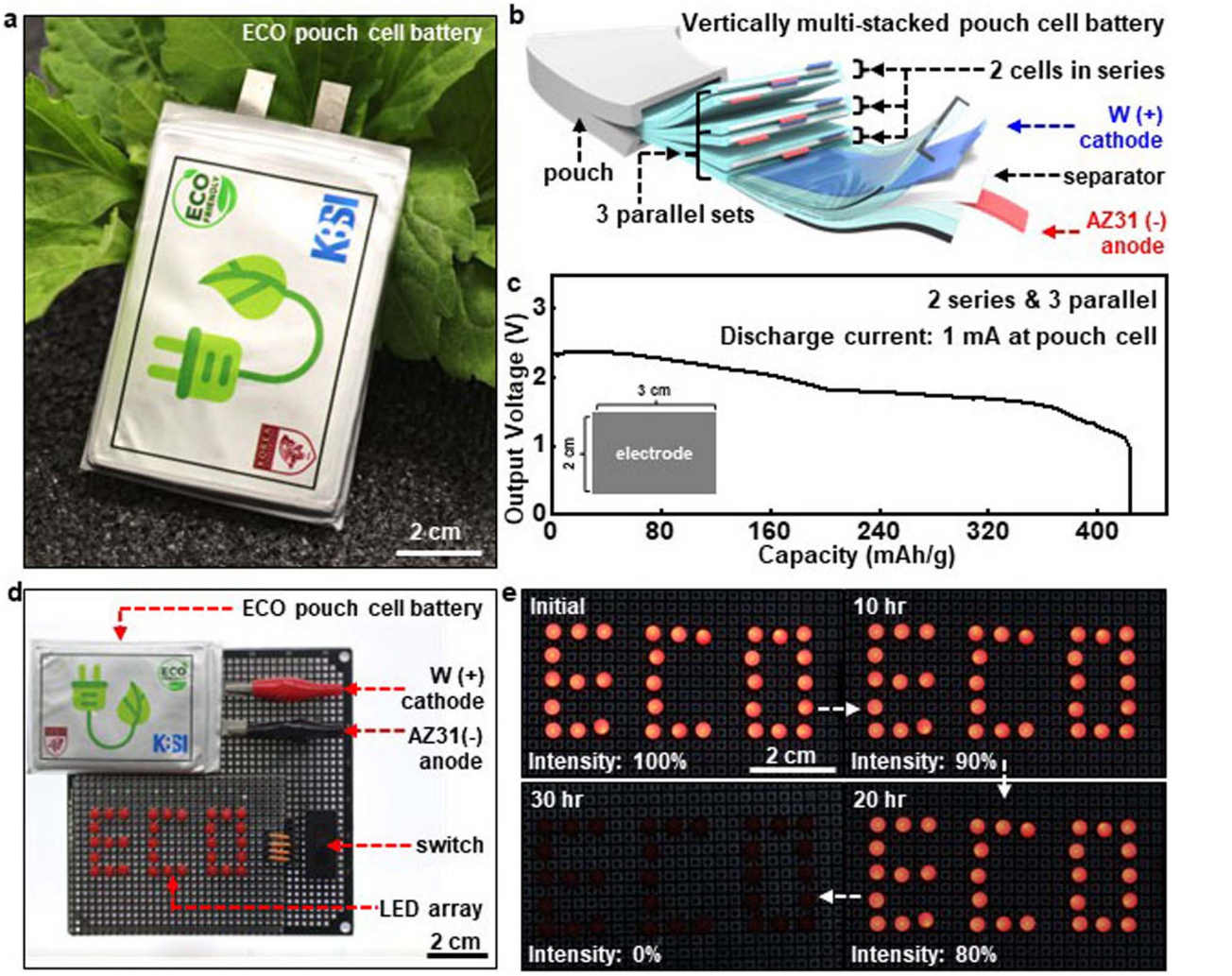

Fig. 3 Biodegradable 'ECO' pouch cells. (a) Optical image of an ECO pouch battery based on the proposed dissolvable metals including AZ31 and W for both the anode and the cathode. (b) Illustration of the structure of the pouch battery constructed with multiple stacking cells formed in series and parallel. (c) Discharge profiles of the pouch battery at a discharge current of 1 mA for the pouch cell. (d) Experimental tests of an integrated system containing the pouch battery that powers light-emitting diodes (LEDs) arranged in the shape of the letters 'ECO'. (e) A set of images of illuminated LED arrays over time while connected to the pouch source.

AZ31 anode and W cathode. The alginate composite electrolyte was composed of sodium alginate (SA) as a polymer matrix, calcium ions (Ca^{2+}) in calcium chloride ($CaCl_2$) solution as a cross-linker, and glycerol as a plasticizer. In the $CaCl_2$ solution, SA underwent cross-linking of polymer chains through the interaction between Ca^{2+} and the carboxylate groups (–COO–) of SA molecules, referred to as ionotropic gelation.[49] However, due to the insufficient mechanical properties of pure alginate, the glycerol plasticizer has been used to improve the mechanical characteristics.[31,50] Here, SAG0, SAG2, and SAG4 refer to SA films blended with glycerol at the weight ratios of 1 : 0, 1 : 2, and 1 : 4, respectively. Fig. 4b shows the strain–stress curves of different alginate composite electrolytes as a function of glycerol concentration. As the glycerol content increased, the elasticity of the composite electrolytes proportionally increased, and SAG4 can be linearly deformed up to 60%. Conductivity gradually increased as the amount of glycerol increased (Fig. 4c). This can be attributed to the presence of glycerol in the alginate matrix, which creates a soft amorphous structure and forms more free spaces for ion transport.[31,50] This reduction of the

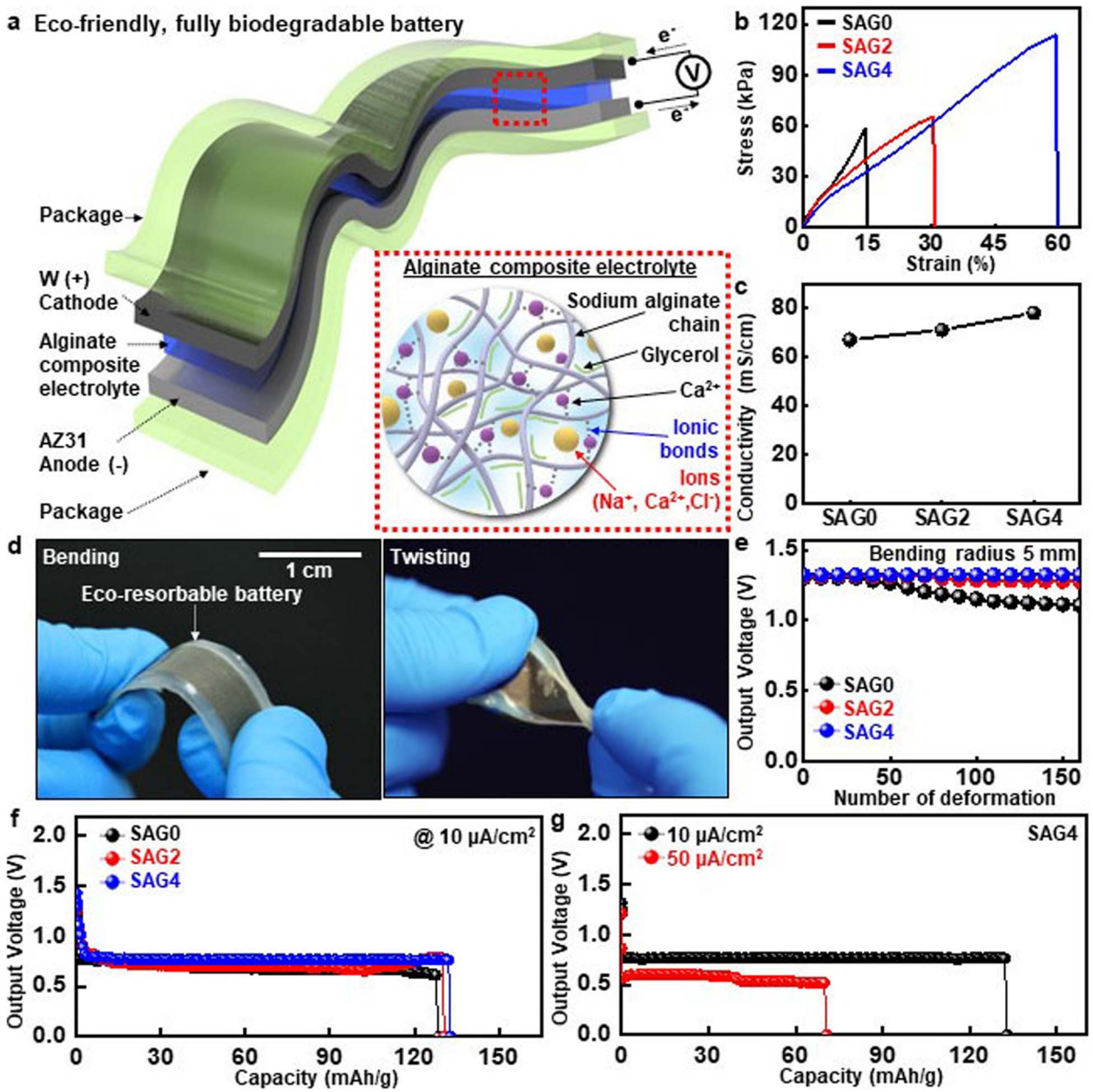

Fig. 4 Soft, stretchable electrolyte-based bioresorbable solid-state battery. (a) Exploded view of a biodegradable solid-state battery and description of alginate-based composite electrolyte. Calcium ions form ionic bonds with the alginate chains, resulting in crosslinking of the sodium alginate when in contact with calcium chloride. (b) Stress–strain curves of alginate composite electrolytes with different concentrations of glycerol. (c) Linear conductivity profile of the electrolytes as a function of glycerol content. (d) Photographs of a soft, dissolvable battery under deformation modes (left, bending; right, twisting). (e) Output voltage characteristics of the batteries against cyclic loads at a bending radius of 5 mm. (f) Discharge curves of the degradable batteries with different concentrations of glycerol within the solid-state electrolyte (at a discharge current density of 10 μA cm^{-2}). (g) Discharge curves of SAG4 with different discharge current densities.

crystalline structure also allows water and other ions to penetrate more easily, accelerating hydrolytic degradation (time-dependent changes in the weight ratios of SAG electrolyte films in Fig. S8†).[51] Fig. 4d depicts the photographs of a solid-state eco-resorbable full-cell battery with packaging layers of polycaprolactone under deformation modes such as bending and twisting. To evaluate the mechanical stability of SAG-based batteries, we measured output voltages under cyclic loadings and recorded stress–strain curves after cyclic deformation at a bending radius of 5 mm (Fig. 4e and S9†). The glycerol incorporated into the alginate-based solid-state electrolytes serves as a plasticizer within the alginate matrix, reducing intermolecular forces between polymer chains and increasing elasticity. As a result, the batteries with SAG2 and SAG4 electrolytes provided stable operation without deterioration in electrical performance, while the SAG0-based one showed a slight decrease in the performance. Fig. 4f presents the discharge behavior of biodegradable solid-state batteries with SAG0, SAG2, and SAG4 electrolytes at a discharge current of 10 μA. The measured discharge capacities were ~128 (SAG0, black), ~130 (SAG2, red), and ~132 (SAG4, blue) mA h g^{-1}, which are consistent with the trend of increased conductivity with the addition of glycerol to the electrolytes, revealing no degradation in the battery performance even with various concentrations of glycerol. Under similar conditions, we recorded the discharge curves of the SAG4 electrolyte-based devices at various currents including 10 and 50 μA cm^{-2} (Fig. 4g). The resulting behavior was quite similar to that in PBS-based liquid electrolytes, and reduced values in output voltage and battery capacity (~70 mA h g^{-1}) were observed as the discharge current density increased to 50 μA cm^{-2} (the time-dependent discharge curve is shown in Fig. S10†).

3 Experimental section

3.1 Electrochemical and morphological evaluation of bioresorbable metals

The electrochemical measurements of bioresorbable metals were performed during semi-immersion of metal foils in a phosphate buffered saline (PBS) solution (pH 7, RT) using a commercial potentiostat (Ivium Technologies, Compact-stat, Netherlands). The open circuit voltage (OCV) of each metal was measured against a commercial standard electrode (Ag/AgCl saturated with KCl), whose potential is +0.197 V *versus* the standard hydrogel electrode (SHE, 0.000 V). A 50 μm thick AZ31 foil (High Broad New Material, China) was used as the anode, and a 50 μm thick W foil (Nilaco, Japan) was used as the cathode. Their potentials against an Ag/AgCl electrode were measured over 10 days and were compared with those of Mg to compare their functional lifetime. Morphological observation was conducted by scanning electron microscopy (SEM, S-4300, Hitachi, Japan), and the metal foils in their as-prepared state and after 24 h immersion in a PBS solution (pH 7, RT) were compared. The discharge behavior of AZ31–W galvanic cells (electrode surface area, 1 cm × 1 cm = 1 cm^2) with PBS solution as an electrolyte was investigated with various current densities using a commercial potentiostat.

3.2 Fabrication of ECO pouch batteries

ECO pouch batteries were fabricated by preparing AZ31 and W foils for electrodes, which were cut into sizes of 2 cm × 3 cm using an ultraviolet (UV) laser marker (MD-U1000C, Keyence, Japan), and glass microfiber filters (Cytiva, China) for the separator, which were cut into sizes of 3 cm × 3.5 cm. Then, AZ31–W cells with PBS solution (pH 7, RT) wetted glass fiber separators were stacked to achieve a high-voltage pouch battery, with each cell being placed in a heat-sealed PCL package to ensure separation from other cells. The individually sealed AZ31–W cells were then assembled into two series and three parallel connections with an external electrode using forge welding. Finally, the whole cells were packaged with biodegradable PCL pouches. To determine the brightness of the ECO LEDs, their luminance was measured using portable luminance meters (MAVO-SPOT 2 USB, GOSSEN, Germany) at a fixed distance of 40 cm from the ECO LEDs. The data were collected through external software (gLux) connected *via* USB.

3.3 Preparation of soft, stretchable bioresorbable electrolytes and their characterization

Pre-cured bioresorbable electrolyte solutions were prepared by dissolving alginic acid sodium salt (SA, Sigma-Aldrich, South Korea) in PBS solution (pH 7) at a concentration of 30 w/v% with continuous stirring at 90 °C for 12 h. An appropriate weight of glycerol (Daejung Chem., South Korea) was added into the prepared SA solutions, respectively, to achieve weight ratios of 1 : 0, 1 : 2, and 1 : 4 (SA : glycerol), and the solutions were stirred at RT for 12 h. Finally, a soft, stretchable biodegradable electrolyte film was formed by immersing the glycerol-added SA solution into a 0.5 M $CaCl_2$ solution at room temperature. Mechanical property measurement was done by using a universal mechanical testing system (Instron 5900 series, Instron, USA) with the sample cut into a dumbbell shape (ASTM D638). The samples were immersed in PBS (pH 7) at room temperature, 37 °C, and 50 °C for biodegradation testing. Each sample was removed every week, rinsed with DI water, and dried using a freeze dryer (TFD 8503, IlShinBioBase, South Korea). The weight ratio was calculated using the formula weight ratio (%) = $W_a/W_b \times 100$, where W_b and W_a are the weights of the samples before and after the immersion, respectively. To determine the ionic conductivity, the electrochemical impedance of the polymer electrolytes was measured in a frequency range of 1 to 106 Hz. A piece of electrolyte was sandwiched between two stainless steel (SUS304) plates. The area (A) was fixed at 1 cm^2, the distance (d) was the thickness of the electrolyte, and the bulk resistance (R) was determined from the intercept with the real axis in impedance spectra. The ionic conductivity (σ) was calculated using the following equation:

$$\sigma = d/(R \times A) \quad (5)$$

3.4 Fabrication of the eco-friendly, fully biodegradable solid-state battery

The eco-friendly, fully bioresorbable solid-state battery was fabricated by cutting AZ31 and W foil with a laser marker for the electrodes of solid-state battery cells. The soft, stretchable

bioresorbable electrolyte films (1 mm-thick) were freshly made just before mechanically stacking the AZ31 foil, electrolyte film, and W foil. Then, the completely stacked cells were encapsulated in a biodegradable PCL package with heat pressing to prevent dehydration under ambient conditions.

4 Conclusion

The concepts, materials, and system designs reported here present biodegradable material-based flexible, eco-friendly battery systems. Comprehensive electrochemical assessments of a magnesium alloy (AZ31) as the anode validated superior voltage outputs and corrosion resistance compared to those of previously employed pure magnesium. The assembly of the proposed materials into the well-known existing pouch cells suggested the potential for a commercial product. The integration of stretchable, biodegradable sodium alginate-based electrolytes with the dissolvable electrodes realized soft, completely bioresorbable solid-state batteries, suitable for power sources of biomedical devices and environment-friendly electronics.

Data availability

The data that support the findings of this study are available from the corresponding author upon reasonable request.

Author contributions

G.-J. K., T.-M. J., D. S., and H. K. contributed equally to this work. G.-J. K., T.-M. J., D. S., H. K., J. C., and S.-W. H. conceived the research and led the experiments with the advice of S. M. Y., S. H., R. K., W. B. H., W.-H. Y., and A. J. B. S. H., C.-H. E. and S. J. C. contributed to the fabrication and characterization of the transient batteries. G.-J. K., T.-M. J., D. S., H. K., J. C., and S.-W. H. co-wrote the manuscript. All authors reviewed and approved the final manuscript.

Conflicts of interest

There are no conflicts to declare.

Acknowledgements

This work was supported by the Korea Institute of Science and Technology (KIST) Institutional Program (2E32501-23-106), the National Research Foundation of Korea (NRF) grant funded by the Korea government (the Ministry of Science, ICT, MSIT) (RS-2022-00165524), the development of technologies for electroceuticals of National Research Foundation (NRF) funded by the Korean government (MSIT) (RS-2023-00220534), the ICT Creative Consilience program through the Institute of Information & Communications Technology Planning & Evaluation (IITP) grant funded by the Korea government (MSIT) (IITP-2024-2020-0-01819), and the Start up Pioneering in Research and Innovation (SPRINT) through the Commercialization Promotion Agency for R&D Outcomes (COMPA) grant funded by the Korea government (Ministry of Science and ICT) (1711198921), the 2024 Hongik University Research Fund, and the Metropolitan Seoul Center at the Korea Basic Science Institute (KBSI) (A412210).

References

1 S. Y. Hong, S. M. Jee, Y. Ko, J. Cho, K. H. Lee, B. Yeom, H. Kim and J. G. Son, *ACS Nano*, 2022, **16**, 2271–2281.
2 S. Kang, S. Y. Hong, N. Kim, J. Oh, M. Park, K. Y. Chung, S.-S. Lee, J. Lee and J. G. Son, *ACS Nano*, 2020, **14**, 3660–3668.
3 D. G. Mackanic, X. Yan, Q. Zhang, N. Matsuhisa, Z. Yu, Y. Jiang, T. Manika, J. Lopez, H. Yan, K. Liu, X. Chen, Y. Cui and Z. Bao, *Nat. Commun.*, 2019, **10**, 5384.
4 X. Chen, H. Huang, L. Pan, T. Liu and M. Niederberger, *Adv. Mater.*, 2019, **31**, e1904648.
5 A. Poosapati, R. B. Ambade and D. Madan, *Small*, 2022, **18**, e2103495.
6 S. Ji, J. Zhu, Y. Yang, G. Dos Reis and Z. Zhang, *Small Methods*, 2024, **8**, e2301021.
7 S. Ji, J. Zhu, Z. Lyu, H. You, Y. Zhou, L. Gu, J. Qu, Z. Xia, Z. Zhang and H. Dai, *J. Energy Chem.*, 2023, **78**, 565–573.
8 W. Song, J. Zhu, B. Gan, S. Zhao, H. Wang, C. Li and J. Wang, *Small*, 2018, **14**, 1702249.
9 J. J. Roy, S. Rarotra, V. Krikstolaityte, K. W. Zhuoran, Y. D.-I. Cindy, X. Y. Tan, M. Carboni, D. Meyer, Q. Yan and M. Srinivasan, *Adv. Mater.*, 2022, **34**, e2103346.
10 M. S. Khan, M. Javed, M. T. Rehman, M. Urooj and M. I. Ahmad, *Sci. Rep.*, 2020, **10**, 16593.
11 Y. Zhang, B. Wang, Q. Cheng, X. Li and Z. Li, *J. Nanosci. Nanotechnol.*, 2020, **20**, 7231–7254.
12 L. Yin, X. Huang, H. Xu, Y. Zhang, J. Lam, J. Cheng and J. A. Rogers, *Adv. Mater.*, 2014, **26**, 3879–3884.
13 X. Huang, D. Wang, Z. Yuan, W. Xie, Y. Wu, R. Li, Y. Zhao, D. Luo, L. Cen, B. Chen, H. Wu, H. Xu, X. Sheng, M. Zhang, L. Zhao and L. Yin, *Small*, 2018, **14**, 1800994.
14 M. Karami-Mosammam, D. Danninger, D. Schiller and M. Kaltenbrunner, *Adv. Mater.*, 2022, **34**, e2204457.
15 X. Huang, H. Hou, B. Yu, J. Bai, Y. Guan, L. Wang, K. Chen, X. Wang, P. Sun, Y. Deng, S. Liu, X. Cai, Y. Wang, J. Peng, X. Sheng, W. Xiong and L. Yin, *ACS Nano*, 2023, **17**, 5727–5739.
16 H. Li, C. Zhao, X. Wang, J. Meng, Y. Zou, S. Noreen, L. Zhao, Z. Liu, H. Ouyang, P. Tan, M. Yu, Y. Fan, Z. L. Wang and Z. Li, *Adv. Sci.*, 2019, **6**, 1801625.
17 H. Sheng, J. Zhou, B. Li, Y. He, X. Zhang, J. Liang, J. Zhou, Q. Su, E. Xie, W. Lan, K. Wang and C. Yu, *Sci. Adv.*, 2021, **7**, eabe3097.
18 Y. Lee, V. K. Bandari, Z. Li, M. Medina-Sánchez, M. F. Maitz, D. Karnaushenko, M. V. Tsurkan, D. D. Karnaushenko and O. G. Schmidt, *Nat. Commun.*, 2021, **12**, 1–10.
19 X. Zhong, Y. Shao, B. Chen, C. Li, J. Sheng, X. Xiao, B. Xu, J. Li, H.-M. Cheng and G. Zhou, *Adv. Mater.*, 2023, **35**, e2301952.
20 H. Lu, J. Hu, X. Wei, K. Zhang, X. Xiao, J. Zhao, Q. Hu, J. Yu, G. Zhou and B. Xu, *Nat. Commun.*, 2023, **14**, 4435.

21 Z. Zheng, X. Zhong, Q. Zhang, M. Zhang, L. Dai, X. Xiao, J. Xu, M. Jiao, B. Wang, H. Li, Y. Jia, R. Mao and G. Zhou, *Nat. Commun.*, 2024, **15**, 753.
22 M. Tsang, A. Armutlulu, A. W. Martinez, S. A. B. Allen and M. G. Allen, *Microsyst. Nanoeng.*, 2015, **1**, 1–10.
23 P. Nadeau, D. El-Damak, D. Glettig, Y. L. Kong, S. Mo, C. Cleveland, L. Booth, N. Roxhed, R. Langer, A. P. Chandrakasan and G. Traverso, *Nat. Biomed. Eng.*, 2017, **1**, 0022.
24 X. Jia, C. Wang, C. Zhao, Y. Ge and G. G. Wallace, *Adv. Funct. Mater.*, 2016, **26**, 1454–1462.
25 J. M. E. Abarro, J. D. Ocon and J. A. D. Del Rosario, *Chem. Eng. Trans.*, 2022, **94**, 151–156.
26 V. Edupuganti and R. Solanki, *J. Power Sources*, 2016, **336**, 447–454.
27 I. Adekanmbi, C. Z. Mosher, H. H. Lu, M. Riehle, H. Kubba and K. E. Tanner, *Mater. Sci. Eng., C*, 2017, **77**, 1135–1144.
28 L. Yin, H. Cheng, S. Mao, R. Haasch, Y. Liu, X. Xie, S.-W. Hwang, H. Jain, S.-K. Kang, Y. Su, R. Li, Y. Huang and J. A. Rogers, *Adv. Funct. Mater.*, 2014, **24**, 645–658.
29 Y.-Q. Sun, W. Fu, Y.-X. Hu, J. Vaughan and L.-Z. Wang, *Tungsten*, 2021, **3**, 245–259.
30 N. Shaari, S. K. Kamarudin, S. Basri, L. K. Shyuan, M. S. Masdar and D. Nordin, *J. Appl. Polym. Sci.*, 2018, **135**, 46666.
31 B. Yavuzyegit, A. Karali, A. De Mori, N. Smith, S. Usov, P. Shashkov, R. Bonithon and G. Blunn, *ACS Appl. Bio Mater.*, 2024, **7**, 1735–1747.
32 D. Kwon, H. Van Pham, P. Song and S. Moon, *Metals*, 2023, **13**, 1150.
33 N. Strigul, *Ecotoxicol. Environ. Saf.*, 2010, **73**, 1099–1113.
34 D. B. Ringelberg, C. M. Reynolds, L. E. Winfield, L. S. Inouye, D. R. Johnson and A. J. Bednar, *J. Environ. Qual.*, 2009, **38**, 103–110.
35 E. Patrick, M. E. Orazem, J. C. Sanchez and T. Nishida, *J. Neurosci. Methods*, 2011, **198**, 158–171.
36 J. L. Greger, *Ciba Found. Symp.*, 1992, **169**, 26–35; discussion 35–49.
37 Y. Song, G. Qin, L. Du, H. Hu and Y. Han, *Arch. Med. Sci.*, 2022, **18**, 195–205.
38 Y. Liu, S. Zheng, N. Li, H. Guo, Y. Zheng and J. Peng, *Sci. Rep.*, 2017, **7**, 40184.
39 S. Wang, C. Du, X. Shen, X. Wu, S. Ouyang, J. Tan, J. She, A. Tang, X. Chen and F. Pan, *J. Magnesium Alloys*, 2023, **11**, 3012–3037.
40 J. Zong, Q. He, Y. Liu, M. Qiu, J. Wu and B. Hu, *Mater. Today Bio*, 2022, **16**, 100368.
41 M. Peuster, C. Fink and C. von Schnakenburg, *Biomaterials*, 2003, **24**, 4057–4061.
42 I. B. Singh, M. Singh and S. Das, *J. Magnesium Alloys*, 2015, **3**, 142–148.
43 Q. Li, W. Xiong, S. Yu, Y. Liu, J. Li, L. Liu, X. Bi, G. Zhu, E. Liu, Y. Zhao and B. Wang, *J. Mater. Sci.*, 2021, **56**, 12789–12802.
44 M. Alvarez-Lopez, M. D. Pereda, J. A. del Valle, M. Fernandez-Lorenzo, M. C. Garcia-Alonso, O. A. Ruano and M. L. Escudero, *Acta Biomater.*, 2010, **6**, 1763–1771.
45 S. Esmailzadeh, M. Aliofkhazraei and H. Sarlak, *Prot. Met. Phys. Chem. Surf.*, 2018, **54**, 976–989.
46 X. Jia, Y. Yang, C. Wang, C. Zhao, R. Vijayaraghavan, D. R. MacFarlane, M. Forsyth and G. G. Wallace, *ACS Appl. Mater. Interfaces*, 2014, **6**, 21110–21117.
47 P. Sun, P. Bai, Z. Chen, H. Su, J. Yang, K. Xu and Y. Xu, *Small*, 2020, **16**, e1906462.
48 T. Zhang, Z. Li, W. Hou and Y. Yang, *Mater. Today Nano*, 2020, **9**, 100070.
49 M. A. Patel, M. H. H. AbouGhaly, J. V. Schryer-Praga and K. Chadwick, *Carbohydr. Polym.*, 2017, **155**, 362–371.
50 O. Hu, G. Chen, J. Gu, J. Lu, J. Zhang, X. Zhang, L. Hou and X. Jiang, *Int. J. Biol. Macromol.*, 2020, **164**, 2512–2523.
51 A. Samir, F. H. Ashour, A. A. A. Hakim and M. Bassyouni, *npj Mater. Degrad.*, 2022, **6**, 68.

